

Effect of Absolute Laser Phase on Reaction Dynamics

A Thesis

Submitted to the Faculty of Science

Ain Shams University

For the degree of Doctor

of Philosophy in Physics

By

Elwallid Shehata Kotb Mohamed Sedik

National Research Center

M.Sc. Physics, Faculty of Science,

Ain Shams University, Cairo, Egypt (1998)

Supervised by

**Prof. Dr. Mohamed Hassan Talaat
Prof. of laser Physics
Faculty of Science
Ain Shams University**

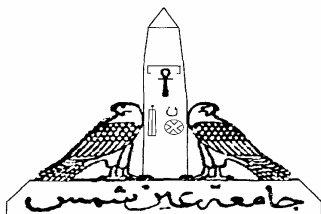
**Prof. Dr. Mohamed Tag El-Din Ahmed Kamal
Theoretical Physics Department
Physics Division
National Research Center.**

2009

To my beloved father, Shehata K. M. Sedik

To my beloved Mother, Settin M. Mazroah

To my beloved Sister, Nagla S. Sedik



Approval Sheet

- **Student Name:** Elwallid Shehata Kotb Mohamed Sedik.
- **Thesis Title:** Effect of Absolute Laser Phase on Reaction Dynamics.
- **Degree:** Doctor of Philosophy.

Supervision Committee

- 1) Prof. Dr. Mohamed Hassan Talaat.
Physics Department, Faculty of Science, Ain Shams University.
- 2) Prof. Dr. Mohamed Tag El-Din Ahmed Kamal.
Theoretical Physics Department, Physics Division, National Research Center.

Higher Studies

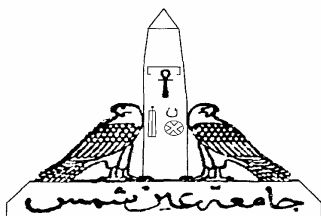
- **Thesis Approval Data:** / / 2010.

University Council Approval

/ / 2010

Faculty Council Approval

/ / 2010



Acknowledgements

I would like to express my sincere thanks to **Prof. Dr. Mohamed Hassan Talaat**, Professor of Laser Physics, Physics Department, Faculty of Science, Ain Shams University for continuous help, sincere advices and for critical revising of the thesis.

I would like to express my sincere thanks to **Prof. Dr. Mohamed Tag El-Din Ahmed Kamal**, Professor of theoretical Physics, Theoretical Physics Department, Physics Division, National Research Center for continuous help, sincere advices and for critical revising of the thesis

I would like to extend my gratitude to Ain Shams University and National Research Center.

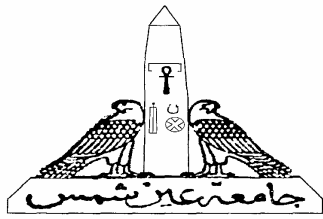
My acknowledgements to:

1. Professor Andre D. Bandrauk, Professor of Chemistry, Universite de Sherbrooke, Quebec, Canada for his encouragement and support during my stay at the university (2003-2006). Many thanks for his assistance and advice in this work.

2. Professor Andre Marie Trambly, Professor of Physics, Physics Department Universite de Sherbrooke, Quebec, Canada is acknowledged for his very strong support and encouragement during my research. He is kind enough to accept volunteering as a member of my supervisory committee, providing advice and suggestions. I am very grateful for his contribution and help specially in using the supercomputer.*

This work would not have been possible without the support of the Physics, Chemistry Department, Sherbrooke University, Quebec, Canada a support for which the Chairs are deeply acknowledged. Many thanks are also due to the Departments administrator and to the Department staff members for giving me every possible personal and administrative help using supercomputer over the years.

- Mammouth clusters that are configured with 872 Dell PowerEdge 750 servers with Intel Pentium 4 3.2 GHz processors and 576 Dell PowerEdge SC1425 servers with 64-bit Intel Xeon 3.6 GHz processors. The clusters run on Linux and provides users with 6.3 TeraBytes of memory and more than 200 TeraBytes of overall disk storage.



Title

Name of student: Elwallid Shehata Kotb Mohamed Sedik

Degree: Doctor of Philosophy in Science in Physics

Department: Physics

Faculty: Science

University: Ain Shams

Graduate Year: 1991

Awarded Degree Year: 2010

Contents

	Page
-List of figures.	I
-List of Tables.	VII
- Abstract.	1
- Summary.	2

Chapter 1

Introduction

Preliminary Note on atom-diatomic reactions	4
1. The F + CH ₄ chemical laser reaction	9
(i). Importance	9
(ii). Experimentally	11
(iii). Theoretically	12
2. The Cl + CH ₄ chemical laser reaction	13
(i). Importance	13
(ii). Experimentally	13
(iii). Theoretically	17
3. $\text{LiH} + \text{CH}_3^+ \rightarrow \text{Li}^+ + \text{CH}_4$	18
(i). Importance	18
(ii). Experimentally	18
(iii). Theoretically	18

Chapter 2

Determination of the reaction path, dipole moment and the Polarizability of the reacting systems $F+CH_4$ and $Cl+CH_4$

2.1. Potential Energy Surfaces.	21
2.2. Reaction path on the potential energy surface.	23
2.3. Multipole Expansion.	27
2.4. Molecular Polarizability.	32
2.5. Ab-initio Calculations (Computational Methods).	36
2.6. Results.	39
2.6.1. Comparison of the Calculated $X+CH_4 \rightarrow HX+\bullet CH_3$ ($X=F, Cl$) Reaction Energetics, Geometries and Electrostatic Properties with Experiment.	39
2.6.2. The structure of the Transition State in the $X+CH_4 \rightarrow HX+\bullet CH_3$ Reaction ($X=F, Cl$).	44
2.6.3. Energy, Dipole Moment, and Polarizability Profiles along the reaction Path.	47
2.6.4. Coincidence of the peaks in dipole moment and polarizability with peaks in the rate of change of geometric parameters along the reaction path.	56
2.7. Normal Modes of vibrations.	60

Chapter 3

Effect of Absolute Laser Phase on Reaction Paths in Laser-Induced Chemical Reactions

3.1. Introduction.	70
3.2. Strong fields and interference effects.	72
3.3. Discussion and Conclusion.	76
3.3.1. Discussion.	76
3.3.2. Conclusion.	83

Chapter 4

Laser Control of reaction paths in Ion-Molecule reactions

4.1. Introduction.	86
4.2. Dressed Potentials-Theory.	87
4.3. Laser Modifications of Ion-Molecule Reactions.	96
4.4. Numerical Results and Discussion.	101

Chapter 5

Laser Induced Surface Crossing in Ion-Molecule Reactions

Raising and Lowering of Potential Energy Surfaces

5.1. Alignment of Molecules in a Laser Field.	107
5.2. Control of Potential Energy- Raising and Lowering Surfaces.	110
5.3. Electron Dynamics in Molecules in the laser field limit.	111
5.4. Results and Discussions.	112

Appendix

Schrödinger equation in the presence of a laser field

A.1. Dressed attractive inverted Morse in the presence of a laser field.	119
A.1.1. Incidence from left.	123
A.1.2. Incidence from right.	129
A.2. Dressed repulsive inverted Morse in the presence of a laser field.	137
A.2.1. Incidence from left.	137
A.2.2. Incidence from right.	143
- References	149
- Arabic Summary	153
- Arabic Abstract	155

List of Figures

	Page
1.1. F+CH ₄ chemical apparatus.	10
2.1. (a) Potential energy surface showing the regions of interest . (b) Minimum reaction Path defining the regions (reactant, transition and product). (c) Potential energy surface showing the regions of interest in skewed coordinates.	25
2.6.A. A display of the reactants, transition structures and products of the two reactions X+CH ₄ → XH+CH ₃ , showing the essential geometric change along the reaction path. See also Table III for details of the geometries. (Angles are in degrees, distances are in Angstroms).	46
2.6.B. (a) Total energies; (b) the F-H'-C angle; and (c) the dipole moment z-component along the reaction path of the F+CH ₄ reaction. (All entries are in atomic units, angles are in degrees).	49
2.6.C. Polarizability along the F+CH ₄ reaction path: (a) α_{zz} , (b) $\alpha_{xx}(=\alpha_{yy})$, (c) average polarizability defined as the 1/3 of the trace of the polarizability tensor ($\frac{1}{3} \sum_{i=x,y,z} \alpha_{ii}$). (All entries are in atomic units).	50
2.6.D. (a) Total energies; (b) the Cl-H'-C angle; and (c) the dipole moment z-component along the reaction path of the Cl+CH ₄ reaction. (All entries are in atomic units, angles are in degrees).	54
2.6.E. Polarizability along the Cl+CH ₄ reaction path: (a) α_{zz} , (b) $\alpha_{xx}(=\alpha_{yy})$, (c) average polarizability defined as the 1/3 of the trace of the polarizability tensor ($\frac{1}{3} \sum_{i=x,y,z} \alpha_{ii}$). (All entries are in atomic units).	55

2.6.F. The change in some key internal geometric coordinates along the reaction path (LEFT) and their respective derivatives (RIGHT) with respect to the reaction path

for the F+CH₄ reaction. (a) LEFT: The H'-C distance, RIGHT: $\frac{d[r(\text{H}'\text{-C})]}{ds}$;

(b) LEFT: The H'-F distance, RIGHT: $\frac{d[r(\text{H}'\text{-F})]}{ds}$; and (c) LEFT: the H'-C-H angle,

RIGHT: $\frac{d[\angle(\text{H}'\text{-C-H})]}{ds}$. (Reaction coordinates are in atomic units, angles are in

degrees, distances are in Å).

58

2.6.G. The change in some key internal geometric coordinates along the reaction path (LEFT) and their respective derivatives (RIGHT) with respect to the reaction path

for the Cl+CH₄ reaction. (a) LEFT: The H'-C distance, RIGHT: $\frac{d[r(\text{H}'\text{-C})]}{ds}$;

(b) LEFT: The H'-F distance, RIGHT: $\frac{d[r(\text{H}'\text{-Cl})]}{ds}$; and (c) LEFT: the H'-C-H angle,

RIGHT: $\frac{d[\angle(\text{H}'\text{-C-H})]}{ds}$. (Reaction coordinates are in atomic units, angles are in

degrees, distances are in Å).

59

2.7.1. Translational frequency determined along the IRP by the method of

Miller et al.,. The translational frequency having negative values corresponds to imaginary frequencies. The translational frequency as a function of the reaction coordinate *s*. It starts in the reactant at -5.4135 a.u. with 57 cm⁻¹ and drops sharply near the transition state zone at 0.1996 a.u. with -3102.6 cm⁻¹ then increasing in the product until it reaches 141.5 cm⁻¹ at 3.7896 a.u.

62

2.7.2. Harmonic vibrational frequencies belonging to the irreducible

representation A₁(ω_1^{A1}), determined along the IRP by the method

of Miller et al.,. The reactive mode (breathing mode) as a function

of the reaction coordinate *s*. It starts in the reactant at -5.4135 a.u. with

3096.5 cm⁻¹ and drops sharply near the transition state zone at 0.0998 a.u.

with 1343.2 cm^{-1} then increasing in the product until it reaches 3990.1 cm^{-1} at 3.7896 a.u. which forms the HF chemical laser.

63

2.7.3. Harmonic vibrational frequencies belonging to the irreducible representation $A_1 (\omega_2^{A_1})$, determined along the IRP by the method of Miller et al.,. The asymmetric mode as a function of the reaction coordinate s . It starts in the reactant at -5.4135 a.u. with 3230.7 cm^{-1} and drops sharply near the transition state zone at 0.0 a.u. with 3130.8 cm^{-1} then increasing in the product until it reaches 3169.4 cm^{-1} at 3.7896 a.u. which forms the CH_3 vibration.

64

2.7.4. Harmonic vibrational frequencies belonging to the irreducible representation $E (\omega_2^E)$, determined along the IRP by the method of Miller et al.,. The spectator modes of CH_4 as a function of the reaction coordinate s . It starts in the reactant at -5.4135 a.u. with 1584.4 cm^{-1} and drops sharply near the transition state zone at 0.0 a.u. with 1513.6 cm^{-1} then decreasing in the product until it reaches 1451.6 cm^{-1} at 3.7896 a.u. which forms the CH_3 vibrations

65

2.7.5. Harmonic vibrational frequencies belonging to the irreducible representation $A_1 (\omega_1^{A_1})$, determined along the IRP by the method of Miller et al.,. The frequency represents the reactive frequency as a function of the reaction coordinate s . It starts in the reactant at -6.8571 a.u. with 3091.3 cm^{-1} and drops sharply near the transition state zone at -0.1998 a.u. with 1273.1 cm^{-1} then increasing in the product until it reaches 2801.8 cm^{-1} at 3.8944 a.u. which gives the HCl vibration.

66

2.7.6. Harmonic vibrational frequencies belonging to the irreducible representation $A_1 (\omega_2^{A_1})$, determined along the IRP by the method of Miller et al.,. The frequency represents the asymmetric frequency as a function of the reaction coordinate s . It starts in the reactant at -6.8571 a.u. with 3217.5 cm^{-1} and drops sharply near the transition

state zone at -0.3996 a.u. with 3126.0 cm^{-1} then increasing in the product until it reaches 3171.4 cm^{-1} at 3.8944 a.u. 67

2.7.7. Harmonic vibrational frequencies belonging to the irreducible representation $E (\omega_1^E)$, determined along the IRP by the method of Miller et al.,. The frequency represents the asymmetric frequency as a function of the reaction coordinate s . It starts in the reactant at -6.8571 a.u. with 3225.2 cm^{-1} and increases near the transition state zone at -0.4971 a.u. with 3265.6 cm^{-1} then increasing in the product until it reaches 3362.9 cm^{-1} at 3.8944 a.u. 68

2.7.8. Harmonic vibrational frequencies belonging to the irreducible representation $E (\omega_4^E)$, determined along the IRP by the method of Miller et al.,. The frequency having negative values corresponds to imaginary frequency. The frequency represents the spectator frequency of CH_4 as a function of the reaction coordinate s . It starts in the reactant at -6.8571 a.u. with -134.4 cm^{-1} and increases near the transition state zone at -0.3996 a.u. with 185.3 cm^{-1} then decreases in the product until it reaches 111.3 cm^{-1} at 3.8944 a.u. 69

3.1. Energy profile for $\text{F}+\text{CH}_4$ along the reaction coordinate, for $I = 1.0 \times 10^{13} \text{ W cm}^{-2}$:
 (a) Triangles: $V(s)$ plus dipole moment contribution, Squares: $V(s)$ plus polarizability contribution at $\phi = 0$, (b) Cross and Dots: $V(s)$ plus both the dipole moment and polarizability contribution at $\phi = 0$ and π respectively. 80

3.2. Energy profile $\text{Cl}+\text{CH}_4$ along the reaction coordinate, for $I = 1.0 \times 10^{13} \text{ W cm}^{-2}$:
 (a) Triangles: $V(s)$ plus dipole moment contribution, Squares: $V(s)$ plus polarizability contribution at $\phi = 0$, (b) Cross and Dots $V(s)$ plus both the dipole moment and polarizability contribution at $\phi = 0$ and π respectively.
 Field-induced bound states are shown at $\phi = \pi$. 81

3.3. Energy profile along the reaction coordinate, for $I = 3.0 \times 10^{13} \text{ W cm}^{-2}$:
 (a) $\text{F}+\text{CH}_4$ surface plus both the dipole moment and polarizability contribution at $\phi = \pi$.
 (b) $\text{Cl}+\text{CH}_4$ surface plus both the dipole moment and polarizability contribution.

Field-induced bound states are shown to have a deep minimum at $\phi = \pi$ as the field intensity is increased. 82

- 4.1. Plot of the potential energy surface of the $\text{Li-H} + \text{CH}_3^+ \rightarrow \text{Li}^+ + \text{CH}_4$ reaction:
 a) repulsive inverted Morse, (It is notable that the reaction lacks a transition state and the reaction proceeds without barrier to form the products.); b) Inverted Morse;
 c) linear dipole moment. 92

- 4.2. The geometries of the reactants, dipolar and polarizability transition states, and products for the $\text{Li-H} + \text{CH}_3^+ \rightarrow \text{Li}^+ + \text{CH}_4$ reaction. The dipole moment magnitude and its direction at each of these points on the reaction path is indicated by the arrow above the ball-and-stick diagrams. The length of the arrow is approximately proportional to the dipole magnitude and its direction points from the negative center to the positive center. 98

- 4.3. a) $A(\gamma)$ as a function of laser parameter γ ; b) γ as a function of E and ω . 103

- 4.4. Transmission coefficient profile T_{\pm} as a function of incident energy for inverted Morse potentials V_{\pm} (see Fig.(1)) respectively in the presence of: (a) $\gamma = 0$, i.e. zero laser field for incident energy (0.00082-0.001 a.u.). (b) $\gamma = -0.09$, $\lambda = 1.03 \times 10^4$ nm, $I = 1.5 \times 10^{14} \text{ W cm}^{-2}$; $\gamma = -0.3$, $\lambda = 2.06 \times 10^4$ nm, $I = 1.1 \times 10^{14} \text{ W cm}^{-2}$; $\gamma = -0.5$, $\lambda = 2.06 \times 10^4$ nm, $I = 2.8 \times 10^{14} \text{ W cm}^{-2}$. 105

5. The ion molecule reaction $\text{LiH} + \text{CH}_3^+ \leftrightarrow \text{Li}^+ + \text{CH}_4$. where θ and ϕ are respectively, the polar and azimuthal angles of the molecular axis with respect to the laser field. 109

- 5.1. Snapshots of the energy profile along the reaction coordinate plus inclusion of only the Dipole moment for $\text{LiH} + \text{CH}_3^+ \rightarrow \text{Li}^+ + \text{CH}_4$. $I = 5 \times 10^{12} \text{ W/cm}^2$.
 a) $\theta = 0.0$, b) $\theta = \pi/4$. 113

- 5.2. Snapshots of the energy profile along the reaction coordinate plus inclusion of only the Dipole moment for $\text{LiH} + \text{CH}_3^+ \rightarrow \text{Li}^+ + \text{CH}_4$. $I = 5 \times 10^{12} \text{ W/cm}^2$.

a) $\theta = \pi/3$, b) $\theta = 2\pi/3$.	114
5.3. Snapshots of the energy profile along the reaction coordinate plus inclusion of only the Dipole moment for $\text{LiH} + \text{CH}_3^+ \rightarrow \text{Li}^+ + \text{CH}_4$. $I = 5 \times 10^{12} \text{ W/cm}^2$. $\theta = \pi$.	115
5.4. Snapshots of the energy profile along the reaction coordinate plus inclusion of only the Dipole moment for $\text{LiH} + \text{CH}_3^+ \rightarrow \text{Li}^+ + \text{CH}_4$. $I = 1 \times 10^{13} \text{ W/cm}^2$. a) $\theta = 0.0$, b) $\theta = \pi/4$.	116
5.5. Snapshots of the energy profile along the reaction coordinate plus inclusion of only the Dipole moment for $\text{LiH} + \text{CH}_3^+ \rightarrow \text{Li}^+ + \text{CH}_4$. $I = 1 \times 10^{13} \text{ W/cm}^2$. a) $\theta = \pi/3$, b) $\theta = 2\pi/3$.	117
5.6. Snapshots of the energy profile along the reaction coordinate plus inclusion of only the Dipole moment for $\text{LiH} + \text{CH}_3^+ \rightarrow \text{Li}^+ + \text{CH}_4$. $I = 1 \times 10^{13} \text{ W/cm}^2$. $\theta = \pi$.	118
A.1. Attractive inverted Morse potential. a) The incidence of the wave is from left. b) The incidence of the wave is from right.	122
A.2. Transmission coefficient profile T_{\pm} as a function of incident energy for inverted Morse potentials V_{\pm} (see Fig.(1)) respectively in the presence of: a) $\gamma = 0$, i.e. zero laser field for incident energy (0.00082-0.001 a.u.). (b) $\gamma = -0.09$, $\lambda = 1.03 \times 10^4 \text{ nm}$, $I = 1.5 \times 10^{14} \text{ W cm}^{-2}$; $\gamma = -0.3$, $\lambda = 2.06 \times 10^4 \text{ nm}$, $I = 1.1 \times 10^{14} \text{ W cm}^{-2}$; $\gamma = -0.5$, $\lambda = 2.06 \times 10^4 \text{ nm}$, $I = 2.8 \times 10^{14} \text{ W cm}^{-2}$.	135
A.3. Plot of the potential energy surface of the $\text{Li-H} + \text{CH}_3^+ \rightarrow \text{Li}^+ + \text{CH}_4$ reaction: repulsive inverted Morse, (It is notable that the reaction lacks a transition state and the reaction proceeds without barrier to form the products.). a) The incidence of the wave is from left. b) The incidence of the wave is from right.	136